International Journal of Heat and Mass Transfer 55 (2012) 1782–1795

Contents lists available at SciVerse ScienceDirect

International Journal of Heat and Mass Transfer

journal homepage: www.elsevier.com/locate/ijhmt

Coiled-tube heat exchanger for High-Pressure Metal Hydride hydrogen storage systems – Part 1. Experimental study

Milan Visaria, Issam Mudawar *

Hydrogen Systems Laboratory (HSL) and Boiling and Two-Phase Flow Laboratory (BTPFL), School of Mechanical Engineering, Purdue University, West Lafayette, IN 47907, United States

ARTICLE INFO

Article history:
Available online 12 December 2011

Keywords:
Fuel cells
Hydrogen storage
Heat exchangers

ABSTRACT

This two-part study explores the development and thermal performance of a coiled-tube heat exchanger for hydrogen fuel cell storage systems utilizing High-Pressure Metal Hydride (HPMH). The primary purpose of this heat exchanger is to tackle the large amounts of heat released from the exothermic hydriding reaction that occurs when the hydrogen is charged into the storage vessel and is absorbed by the HPMH. The performance of heat exchanger was tested using 4 kg of $Ti_{1.1}CrMn$ at pressures up to 280 bar. Tests were performed to assess the influence of different operating conditions on the effectiveness of the heat exchanger at removing the heat in a practical fill time (time required to complete 90% of the hydriding reaction). It is shown that distance of metal hydride particles from the coolant tube has the most dominant influence on hydriding rate, with particles closer to the tube completing their hydriding reaction sooner. Faster fill times were achieved by reducing coolant temperature and to a lesser extent by increasing pressurization rate. By comparing tests with and without coolant flow, it is shown that the heat exchanger reduces fill time by 75% while occupying only 7% of the storage pressure vessel volume. The second part of this study will present a 3D computational heat transfer model of the storage vessel and heat exchanger, and compare the model predictions to the experimental data.

1. Introduction

Despite its high energy content by mass, hydrogen has very low density. This makes the task of storing and transporting an adequate amount of hydrogen in an automobile fuel cell (to ensure an acceptable travel distance between filling stations) quite elusive. Different methods have been proposed to tackle this problem, including storing the hydrogen as a very high-pressure gas, very low temperature liquid, or in solid form by undergoing a chemical reaction in chemical hydrides, metal hydrides, or cryo-adsorbents [1–12]. Each of these storage options provides unique advantages but poses design challenges as well. This study concerns the use of High-Pressure Metal Hydrides (HPMHs) to store the hydrogen.

HPMHs that have been proposed for hydrogen storage possess higher volumetric storage capacity compared to most other storage techniques [4–5,10]. Hydrogen storage and subsequent release to the fuel cell are achieved by two processes, hydriding and dehydriding. The hydriding process is achieved when hydrogen gas at a filling station is supplied into the automobile's storage system by reacting with the metal alloy to produce metal hydride. The dehydriding process is achieved when the hydrogen gas is released from the metal hydride to the fuel cell. These processes are reversible and can be achieved at an acceptably high pressure and relatively low temperature. The present study concerns the hydriding reaction of HPMHs.

Hydriding is a kinetically-driven, temperature-dependent exothermic reaction that generates large amounts of heat. For HPMHs like $Ti_{1.1}CrMn$ that possess fast reaction kinetics, the process is thermally limited. In other words, the factor that limits the rate of reaction is the metal hydride temperature. At a given pressure, faster hydriding rates (needed to ensure an acceptably short fill time) can be achieved only by lowering the metal hydride temperature. Thus, during the filling of hydrogen into the automobile, it is necessary to quickly remove the heat released during the exothermic hydriding reaction and maintain lower hydride temperatures. On the other hand, heat must be added during the endothermic dehydriding reaction to increase hydrogen release rate and meet a wide range of vehicle loads. Thus, the heat exchanger constitutes the most crucial component of a HPMH storage system.

The hydrogen storage system in mobile applications like automobiles must satisfy two important criteria. First, it must allow for quick fueling (loading) and release (unloading) of sufficient quantities of hydrogen gas. This requires high heat transfer rates during both hydriding and dehydriding. Second, the heat

* Corresponding author. Tel.: +1 765 494 5705; fax: +1 765 494 0539.
E-mail address: mudawar@ecn.purdue.edu (I. Mudawar).
URL: https://engineering.purdue.edu/BTPFL (I. Mudawar).

0017-9310/$ - see front matter © 2011 Elsevier Ltd. All rights reserved.
doi:10.1016/j.ijheatmasstransfer.2011.11.035

Nomenclature

C_a	hydriding constant (s^{-1})
E_a	activation energy (J/mol-H_2)
F	fraction of completion of reaction
ΔH_r	enthalpy of reaction (J/mol-H_2)
MW	molecular weight
P	pressure
P_{eq}	equilibrium pressure
P_o	ambient pressure
P_{sys}	operating (system) pressure
$\dot{q}'''$	volumetric heat generation rate (W/m^3)
R	universal gas constant (8.314 J/mol K)
ΔS	entropy of reaction (J/mol-H_2 K)
t	time
T	temperature
wt%	hydrogen to metal hydride mass ratio when completely hydrided

Greek symbols

ρ	density
ϕ	porosity

Subscripts

eq	equilibrium
H_2	hydrogen
MH	metal hydride
sys	system

exchanger and its components must occupy minimal volume to allow for larger quantities of metal hydride and, hence, hydrogen to be stored. In other words, the storage vessel must possess high volumetric and gravimetric efficiencies. In general, modifying the heat exchanger design to increase one of these efficiencies tends to compromise the other. Hence, the heat exchanger design must be optimized to be compact while still achieving short fill times.

The two main bottlenecks in the design of an on-board hydrogen storage system using metal hydrides are the development of (a) materials with high hydrogen storage capacity, and (b) compact storage vessels that achieve short hydrogen fill times. While researchers continue to pursue new storage materials, the design of an effective heat exchanger for the storage vessel has gained increasing attention in recent years. The majority of heat exchanger studies have been focused on low-pressure metal hydride systems using $LaNi_5$, with operating pressures and temperatures around 10 bar and 70 °C, respectively [7,14–18]. A variety of heat exchanger designs have been proposed, including external cooling of the storage pressure vessel with a coolant jacket [6,7] tube-fin heat exchangers with circular fins [17], plate-fin heat exchangers with different fin geometries [6,8–14], spiral-tube heat exchangers with and without fins [7,15–16], and heat exchangers with aluminum foam [17–18]. Several of these studies also involved improving heat transfer performance by mixing high thermal conductivity additives like aluminum powder in the metal hydride.

Only a few studies have focused on developing hydrogen storage systems that employ HPMHs. Pourpoint et al. [9] developed a tube-fin prototype heat exchanger that was tested with 93 g of $Ti_{1.1}CrMn$. Mori and Hirose [11] tested a full-size $Ti_{1.1}CrMn$ hydrogen storage system at 350 bar. They cooled the HPMH using an aluminum heat exchanger that achieved 80% completion of the hydriding reaction in 5 min. However, they did not provide details of the construction or operating conditions of their heat exchanger. Visaria et al. [19–20] designed and tested a prototype heat exchanger with 2.65 kg of $Ti_{1.1}CrMn$. Their design consisted of a liquid cooling U-tube from which a network of fins extending into a bed of HPMH powder inside the storage pressure vessel. The heat exchanger occupied 29% of the pressure vessel volume and achieved 90% completion of the hydriding reaction in only 4 min 40 s.

The primary objective of the present study is to explore the performance of different type of heat exchanger that maximizes hydrogen storage capacity while achieving practical fill times. In this first part of a two-part study, the performance of the heat exchanger is assessed experimentally and the effects of various operating parameters on the hydriding reaction are investigated. The second part [21] will compare the experimental results to predictions of a three-dimensional computational heat transfer model of the heat exchanger.

2. Storage vessel construction and assembly

2.1. Overall construction of storage vessel

The containment test vessel constructed for storing the HPMH powder also houses the heat exchanger and instrumentation required to measure the hydride temperatures. The 355.6 mm (14-in) long containment vessel is inserted along a 101.6 mm (4-in) pressure vessel. The containment vessel consists of a thin-walled cylinder with two cover plates that houses the $Ti_{1.1}CrMn$ powder. Liquid flows through a coiled tube that is embedded in the powder inside the storage vessel to provide cooling during the hydriding reaction and heating during the dehydriding reaction to the surrounding hydride powder. Following are details of the construction of the major components and the storage vessel and its assembly.

2.2. Coiled coolant tube

The approach in designing a heat exchanger for a HPMH storage system is strongly influenced by whether the primary function of the heat exchanger is to achieve a short fill time (*i.e.*, faster heat transfer rate) or greater storage efficiency. The heat exchanger described in [19–20] was specifically tailored to achieving short fill times. This was accomplished with the aid of a network of fins that extended from a cooling tube and were distributed within the powder. Heat transfer effectiveness was maximized by providing localized finning everywhere within the powder. The use of fins reduced the volume available inside the storage vessel for the hydride powder and therefore the hydrogen in favor of a shorter fill time.

The primary goal with the present heat exchanger design is to maximize volumetric storage efficiency by significantly reducing heat exchanger volume. Here, fins are eliminated, and the coolant tube itself is strategically coiled within the metal hydride powder to achieve close proximity to the powder everywhere within the storage vessel.

Fig. 1 shows an isometric and detailed views of the present coiled-tube heat exchanger. The seamless 316 stainless steel cooling tube has an outer diameter of 9.5 mm and wall thickness of 1.65 mm. The tube was formed on a CNC roll-bending machine into a coil 79.2 mm in diameter and a pitch of 24.4 mm. The coil dimensions are based on findings from a previous study concerning the

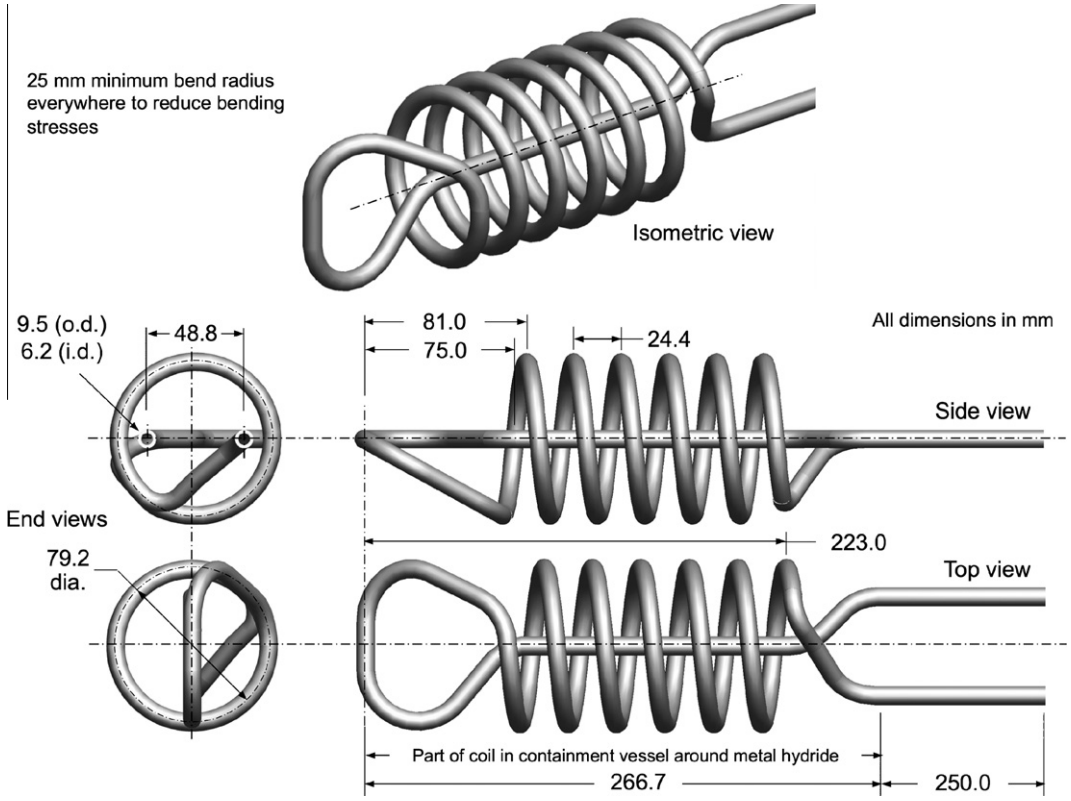

Fig. 1. Isometric view and detailed drawings of coiled coolant tube.

design of HPMH heat exchangers [10]. Predictions of a 1-D model showed that, to achieve practical fill times (~5 min) with $Ti_{1.1}CrMn$, the farthest distance of the hydride powder from the cooling tube should be no greater than 10 mm. However, because of bending stress limits for the coil under 280 bar of external pressure during the actual tests, the coil could provide a maximum distance of only 15 mm. Actually, the 3-D geometry of the coil provides better cooling than estimated by the 1-D model. The cooling tube consists of straight sections on both ends, followed each by bends leading to the middle spiral coils. The straight ends facilitate the use of standard tube fittings to guard against potential leaks, which can be especially problematic in high-pressure applications.

To reduce bending stresses, the radius at each bend is maintained to no less than 25 mm. Also, after manufacturing, the coil was heat treated to relieve bending stresses. This was achieved by heating the tube in a furnace at 400 °C for 2 h, followed by air-cooling to ambient temperature. This heat treatment gave a copper-colored external appearance to the stainless steel coil. The tube used for coiling is rated for 442 bar of internal pressure. Since the coil was subjected to an external pressure of 280 bar during the actual tests, the coil was hydro tested following the heat treatment to at an external pressure of 410 bar.

2.3. Thermocouple support tubes

Metal hydride temperatures are measured using type-T thermocouples placed at 16 different locations. The thermocouple wires are routed to the desired locations using 6.35 mm o.d. stainless steel support tubes. Figs. 2(a) and (b) show details of the support tubes attached to the cover plates on the U-bend (left) side and coolant inlet/outlet (right) side of the containment vessel, respectively. Extending radially from each support tube are eight 1.6 mm o.d. stainless steel tubes of different lengths that are brazed 19 mm apart onto the main support tube but at different orientations. These smaller tubes are strategically positioned to capture the transient thermal response of the metal hydride at varying distances from the cooling tube. A bundle of eight pairs of thermocouple wires is fed into the main tube through an oval cavity at the lower end of each tube as shown in Fig. 2. Each of the smaller tubes then carries a pair of thermocouple wires ending in an exposed thermocouple junction protruding 2 mm from the tip of the tube. The thermocouple wires are secured to each tube with the aid of low conductivity epoxy as shown in the inset in Fig. 2(a). Care is taken to ensure that the thermocouple junction is exposed and directly in contact with the metal hydride. The oval cavity and other openings in each of the main support tubes is sealed with epoxy around the thermocouple wires to prevent the metal hydride powder from entering the tube. Both the main and smaller support tubes provide sufficient rigidity to prevent any displacement of thermocouple junctions during the assembly or due to expansion of the powder while testing.

2.4. Cover plates

The containment vessel is sealed by two cover plates, one on the U-bend (left) side and the other on the coolant inlet/outlet (right) side. The cover plates are made from 304 stainless steel and have diameters slightly smaller than the i.d. of the containment vessel, so that they could fit inside the containment vessel. A pair of O-rings on each cover plate is used to prevent leaks between the cover plate and the containment vessel. Additionally, each cover plate is attached to the containment vessel with the aid of three set screws. The cover plate on the U-bend side has four fittings, two for check valves, one for a thermocouple feed-through, and one for the main thermocouple support tube. The cover plate on the coolant inlet/outlet side has five fittings, two for check valves, two for the coolant tube, and one for a thermocouple feed-through.

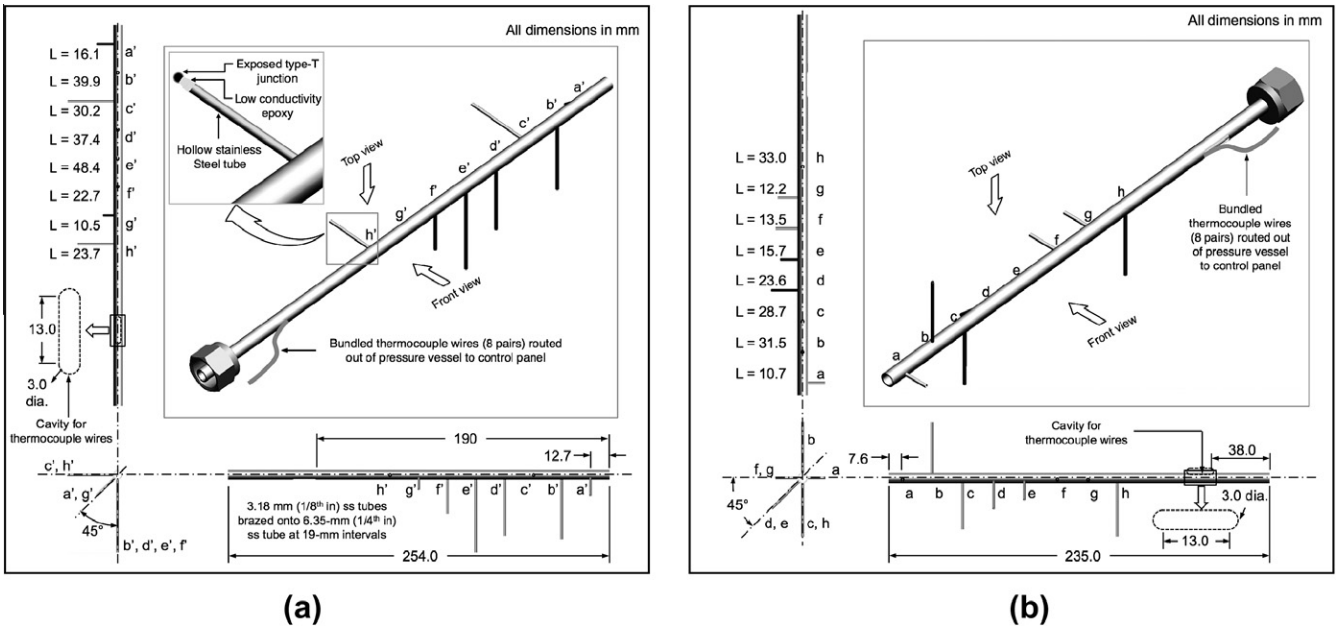

Fig. 2. Isometric views and detailed drawings of thermocouple support tubes attached to cover plates of storage vessel on (a) U-bend (left) side and (b) coolant inlet/outlet (right) side of coolant tube.

In addition, because of limited space, a hex nut is welded on the inner surface of each cover plate to hold the main thermocouple support tube in place. The pair of check valves attached to each cover plate permit flow in opposite directions. They perform the dual function of preventing air from entering the storage vessel (while the vessel is being transported from a glove box to the test cell, as discussed later), and allowing hydrogen gas to flow in and out during the tests. A circular cavity in each cover plate houses a sintered 316 stainless steel diffuser plate with 30% porosity and 10 micron pore size. The purpose of these plates is to help evenly distribute hydrogen gas flow into the vessel while preventing the hydride powder from leaking out. Additional filtering is provided by sheets of filter paper placed on the inner side of each cover plate, held in place by set screws.

2.5. Thermocouple Placement

As discussed earlier, two main thermocouple support tubes, each carrying eight pairs of thermocouple wires, are attached to the cover plates. Shown in Fig. 3 is the placement of the support tubes and locations of thermocouple junctions relative to the coil. The smaller thermocouple support tubes have different lengths and are attached radially to the main tube but at different orientations. With lengths ranging from 1 to 15 mm, and the different orientations, the smaller support tubes provide the desired 3-D placement of thermocouple junctions relative to the coil. There are also practical considerations that influence the lengths and positions of these tubes. Although not examined in this study, the placement of thermocouples at different elevations inside the

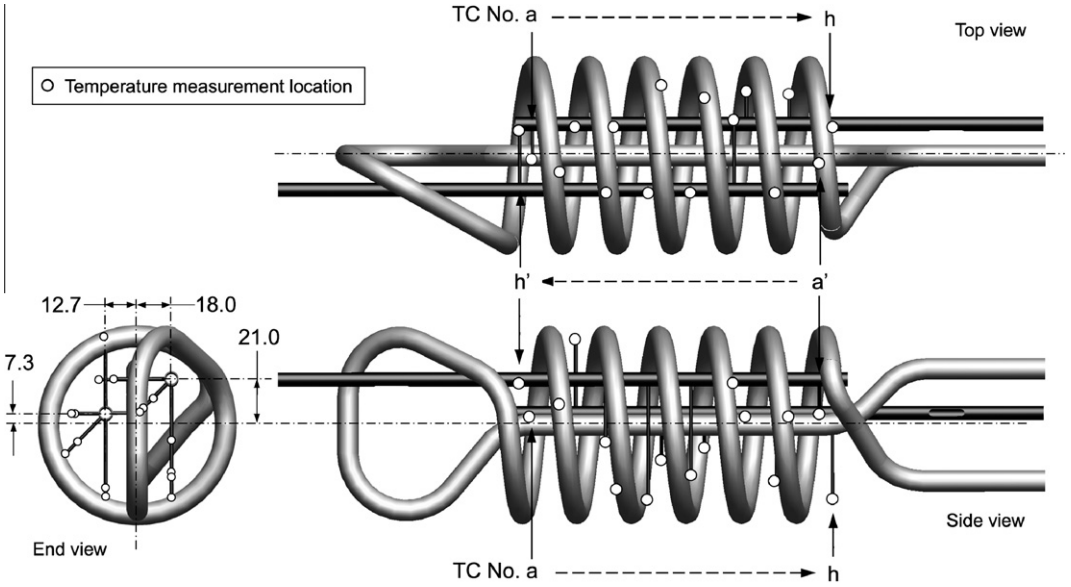

Fig. 3. Location of thermocouples relative to coiled coolant tube.

hydride powder allows the study of any effects of gravity-induced powder density variations on the hydriding process. Temperatures are measured only along the coiled portion of the cooling tube. Temperatures measured by thermocouples attached to the cover plate on the coolant inlet/outlet side are designated as *a*–*h*, and those on the U-bend side *a*′–*h*′.

2.6. Heat exchanger assembly

For the purpose of both experimental and computational study, it is crucial that the distance of each thermocouple from the coolant tube be precisely ascertained. Towards this end, a CAD model of the heat exchanger assembly, Fig. 4, was generated using dimensions of all components and relative locations of thermocouples. Key dimensions of the actual assembly, which is shown in the photo is Fig. 4 housed in a temporary transparent cylindrical plastic housing, and the CAD model are carefully compared to ensure that precise details of the assembly are achieved. The CAD model proved very useful in measuring the distance between thermocouples and the coolant tube at locations that are hard to access.

2.7. Metal hydride activation and containment vessel filling

At 500 bar, the hydride temperature for $Ti_{1.1}CrMn$ is limited to 85 °C, making this material a very suitable candidate for hydrogen storage in automobiles as well as for the present experiments. In this study, pressure was limited to 280 bar, which corresponds to a peak metal hydride temperature of only 50 °C.

$Ti_{1.1}CrMn$ is supplied in non-reactive state, with a particle size of a few hundred microns and having a thin oxidized outer surface. For the hydride to become reactive and absorb hydrogen, it needs to be broken into very fine particles in order to increase both surface area and number of absorption sites. Hydride 'activation' is achieved by subjecting the $Ti_{1.1}CrMn$ powder to repeated cycles of cooling in high pressure hydrogen gas and heating at low pressure (vacuum) as discussed in [20]. Once activated, its kinetic and thermal properties (discussed in [21]) are measured before the hydride is filled into the containment vessel. Activated metal hydride is highly reactive and readily ignites in the presence of oxidizers such as air or water. Hence, utmost care is exercised during its handling. It is stored in multiple plastic bags secured in sealed aluminum cans in an argon-filled glove box where less than 0.1 ppm of O_2 and H_2O are maintained.

All components of the containment vessel and heat exchanger must be transported into the same glove box, where the vessel is filled with the metal hydride powder. The filling process yields a hydride packing density of 2.2 g/cc. The containment vessel is fully assembled inside the glove box before being transported into a separate cell for testing.

3. Experimental procedure

3.1. Hydrogen and coolant flow loops

Shown in Fig. 5 is a simplified schematic of the test facility. Transported from the glove box, the assembled containment vessel is carefully transported inside a sealed plastic casing into the adjoining secure test cell. The storage vessel is slid inside a pressure vessel made from 304 stainless steel and rated for 410 bar. The coolant lines are then connected to the coil heat exchanger and the hydrogen lines to the pressure vessel. Temperature and pressure sensors (not shown in Fig. 5) are routed out of the pressure vessel and connected to an external instrumentation panel. End flanges are used to seal the pressure vessel. Once the containment vessel is secured and the pressure vessel sealed, a positive

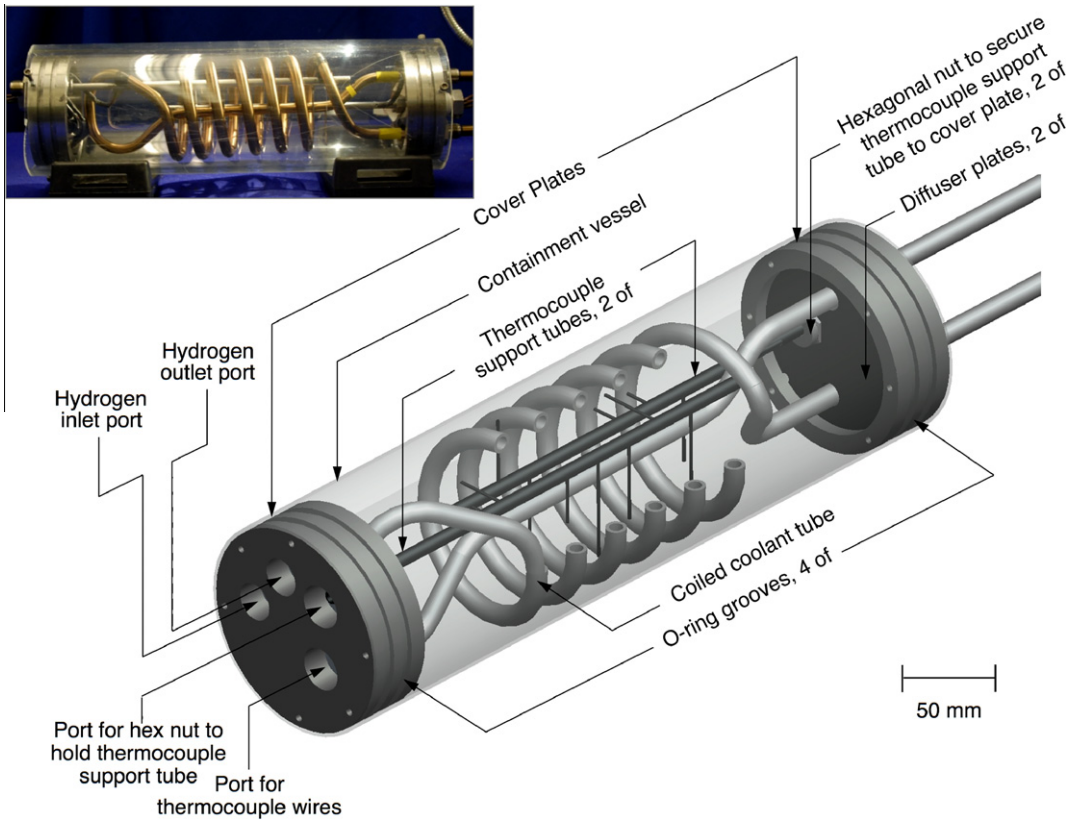

Fig. 4. Detailed 3-D rendering of containment vessel/heat exchanger assembly.

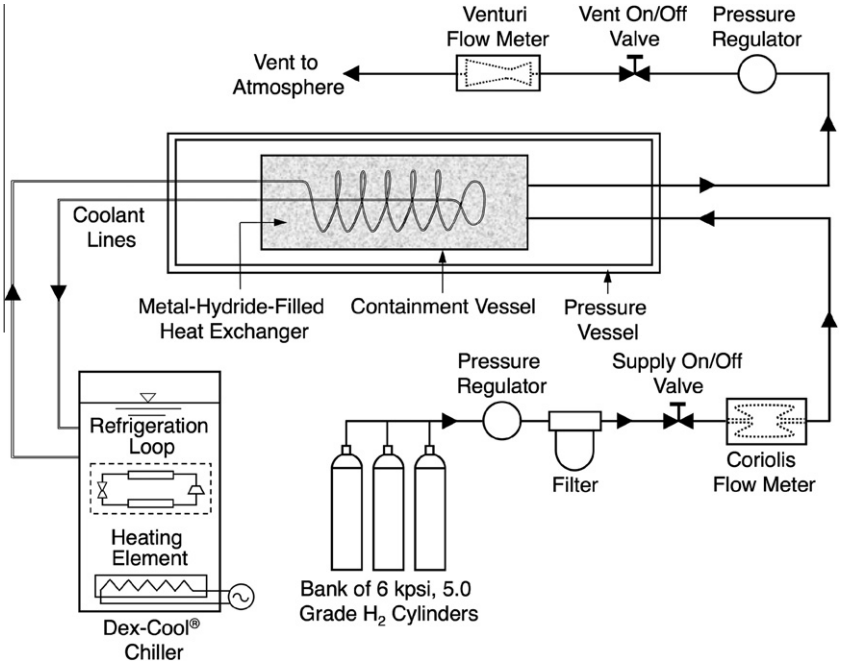

Fig. 5. Schematic diagram of test facility.

hydrogen pressure of 7 bar is maintained to prevent air from entering the system in the event of a leak.

The coolant supplied through the heat exchanger coil is Dex-cool®, a commercial automotive anti-freeze. The coolant lines are connected externally to an air-cooled chiller capable of delivering up to 17 lpm of coolant at temperatures ranging from 0 to 25 °C.

The hydrogen is supplied from cylinders containing 5.0 grade hydrogen gas at 410 bar. An electronically controlled pressure regulator is used to supply the hydrogen to the pressure vessel at the desired flow rate. A filter is placed in the supply line to remove any impurities larger than 10 μm from the incoming hydrogen gas. On/off valves in the supply and vent lines are used to isolate the pressure vessel from the rest of the system when no experiments are being performed or in the vent a leak is detected. A Coriolis flow meter measures the flow of hydrogen entering the pressure vessel while a venturi flow meter in the vent line measures the flow rate of exiting hydrogen gas. A regulator in the vent line controls the hydrogen outflow.

During the experiments, the following parameters are continuously monitored and recorded: (a) temperature and flow rate of the coolant, (b) inflow and outflow rates of the hydrogen gas, (c) temperature of hydrogen gas as it enters the pressure vessel, (d) pressures at different locations in the flow loop and in the pressure vessel, (e) metal hydride temperatures, and (f) hydrogen level at three locations in the test cell (to detect any leaks).

3.2. Pressurization profile

In metal hydrides, the rate of hydriding is governed by the amount by which the system pressure exceeds the hydride's equilibrium pressure. The temperature-dependent equilibrium pressure is given by the van't Hoff equation [10],

$$P_{eq} = P_o exp\left(\frac{\Delta H_r}{RT} - \frac{\Delta S}{R}\right). \quad (1)$$

This relationship between the hydride's equilibrium pressure and temperature for $Ti_{1.1}CrMn$ during hydriding is plotted in Fig. 6 (this curve is different for the dehydriding reaction due to hysteresis). Notice how the equilibrium pressure increases exponentially with increasing hydride temperature. At any temperature, the hydride can react with hydrogen only when P_{sys}/P_{eq} exceeds unity, and, the greater this pressure ratio, the faster is the reaction rate. Thus, to increase hydriding rate, either the system pressure must be increased or the equilibrium pressure lowered by reducing the hydride temperature. When the system pressure is at 280 bar (maximum pressure in the present experiments), the hydride will react until it reaches the temperature corresponding to the same value of equilibrium pressure, *i.e.*, 50 °C. The reaction then stops and cannot be re-initiated until the hydride is cooled below 50 °C. Thus, the peak system pressure sets an upper limit on hydride temperature.

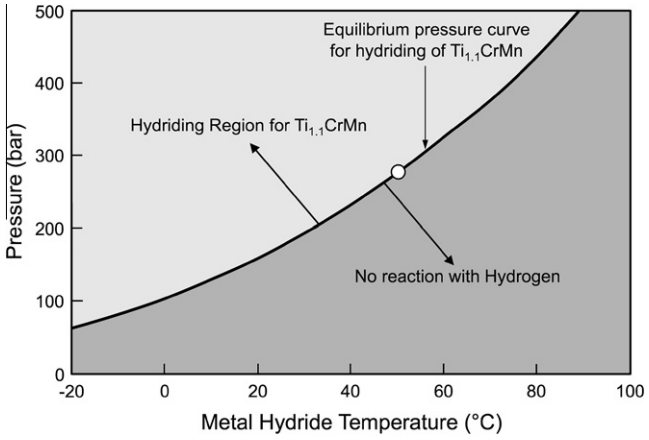

Fig. 6. Variation of equilibrium pressure during hydriding of $Ti_{1.1}CrMn$ with temperature.

Fig. 7 shows the pressurization profile during a typical test. Before starting the test, the coolant is set to desired flow rate and temperature. While the coolant is reaching the desired temperature, manual leak checks are performed throughout the flow loop at 35 and again at 70 bar. If any leak is detected, the system is

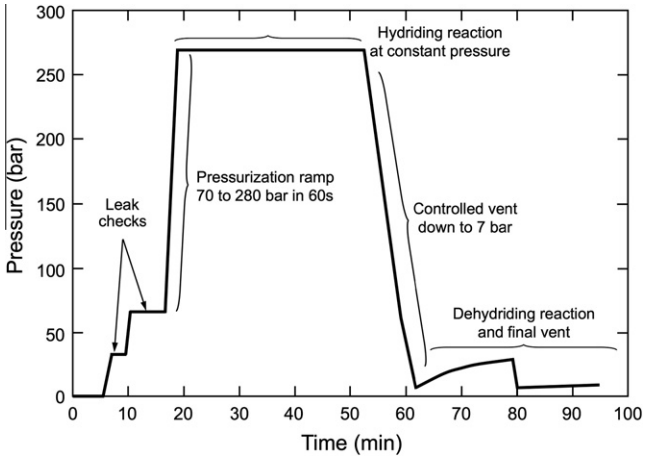

Fig. 7. Pressurization profile during a typical test.

depressurized and the leak fixed. Once the coolant reaches the desired temperature and leak checks are performed, a pressurization ramp is initiated, which, for the case shown in Fig. 7, corresponds to an increase in pressure from 70 to 280 bar. During this ramp, the supply valve is kept open and the vent valve closed. As the pressure increases, the hydride begins to react with the hydrogen and releases heat. The supply valve is kept open at the end of the pressurization to maintain hydrogen pressure. Closing this valve will cause pressure to drop due to both the cooling and the hydrogen absorption caused by the hydriding reaction.

When the hydriding reaction is completed and hydride temperatures are uniform, the supply valve is closed and the pressure vessel isolated. Completion of the hydriding reaction is indicated by a fast drop in the hydride temperatures and appreciable reduction in hydrogen flow into the pressure vessel. Dehydriding is initiated by lowering the pressure, which is achieved by opening the vent valve to release hydrogen at a controlled rate. The dehydriding process can be accelerated by increasing the hydride temperature, which is achieved by heating the coolant to 25 °C. Due to hysteresis, dehydriding does not commence once the pressure is reduced. In fact, the endothermic dehydriding reaction starts below 100 bar, evidenced by a sharp drop in the hydride temperatures. If the pressure vessel is isolated at this stage by closing the vent valve, an increase in pressure, caused by the hydrogen release, will be detected, as seen in Fig. 7 just after 60 min. The test is terminated when the dehydriding process is completed and metal hydride temperatures are uniform. The metal hydride is secured by isolating the pressure vessel and storing it in a positive pressure of 7 bar until the next test.

4. Experimental results

4.1. Summary of experiments

Table 1 shows a summary of four tests that were performed with the coiled-tube heat exchanger. In tests 1–3, pressure was increased from 70 to 280 bar in 60 s, while in test 4 the pressure was increased slowly over 300 s. Coolant temperature was 2.5 °C for test 1, 21.0 °C for test 2, and 4.5 °C for test 4. Since coolant flow rate has minimal effect on the hydriding process [10], its effects were not examined in this study. Similar coolant flow rates were therefore used in tests 1, 2 and 4. Before initiating these three tests, the coolant was supplied to the coiled tube until it reached the desired temperature. In the absence of hydrogen supply, the hydride reached an initial temperature close to that of the coolant. Test 3 was performed in absence of any coolant flow to ascertain the overall merits of employing a heat exchanger.

Table 1
Operating parameters for tests performed.

Operating parameters for tests performed.				
Test No.	Pressurization profile	Coolant flow rate	Coolant temp. (°C)	Avg. initial temp. (°C)
1	70–280 bar in 60 s	11.5 lpm	2.5	4.5
2	70–280 bar in 60 s	14.2 lpm	21.0	20
3	70–280 bar in 60 s	no coolant flow		17
4	70–280 bar in 300 s	12.0 lpm	4.5	5.5

4.2. Metal Hydride temperature profiles

Fig. 8 shows the pressure vessel pressure, metal hydride temperatures and mean coolant temperature (average of coolant's inlet and outlet temperatures, which were typically within 1.5 °C) for the entire duration (hydriding and dehydriding) of test 1. Temperatures measured by only thirteen thermocouples (a–h, a'–c', e' and h') are shown because the three remaining thermocouples (d', f' and g') stopped functioning during the tests apparently due to breakage of thermocouple wires during assembly.

Once the coolant reached the desired temperature, the vessel was pressurized with hydrogen gas. As the pressure was increased, heat was generated due to both the hydriding reaction and pressurization heating. Those two heating effects are evident from the following expression for rate of volumetric heat generation [10],

$$\dot{q}''' = \frac{dF}{dt}\frac{(wt\%)\rho_{MH}}{MW_{H_2}}\Delta H_r + \phi\frac{dP}{dt}. \quad (2)$$

The first right hand side term in Eq. (2) represents the heating caused by the hydriding reaction, which contributes over 90% of the total heat generation rate. The heat generation caused the metal hydride temperature to rise, reaching peak levels at the end of the pressurization ramp at 280 bar. From that point, the pressure was maintained at 280 bar by keeping the hydrogen supply valve open until the hydriding reaction reached completion. As the metal hydride continued to react with the hydrogen, it was also being cooled by the heat exchanger, causing its temperature to decrease. The hydriding rate is related to the cooling rate by the following relation [22],

$$\frac{dF}{dt} = C_a \exp\left(\frac{-E_a}{RT}\right) ln\left(\frac{P}{P_{eq}}\right)(1-F), \quad (3)$$

where F is the fraction of completion of the hydriding reaction. Higher heat transfer rates increase the hydriding rate by lowering both the hydride temperature and equilibrium pressure.

As shown in Fig. 8 for test 1, hydride particles at locations g, c' and h reached the highest temperatures and had the slowest temperature decay rate. On the other hand, particles at a, a' and b' reached much lower temperatures and cooled faster. There appears to be obvious similarities among certain temperature profiles, which allows profiles of different thermocouples to be grouped together based on their distance from the coolant tube.

A simple method is devised to assess the proximity of a thermocouple from the coolant tube. As shown in Fig. 9, a single thermocouple assumes different distances from different parts of the coolant tube. These distances are compared to identify the shortest. This shortest distance provides an approximate measure of

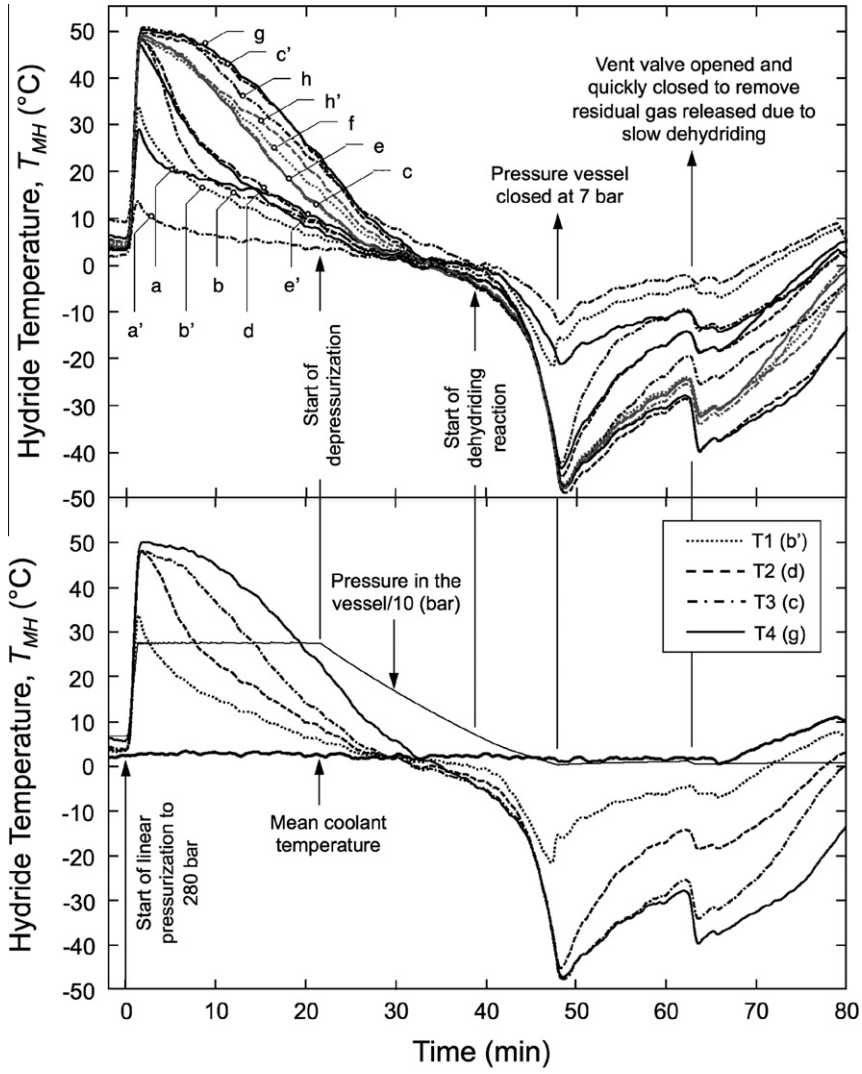

Fig. 8. Temperature profiles during the entire duration of test 1.

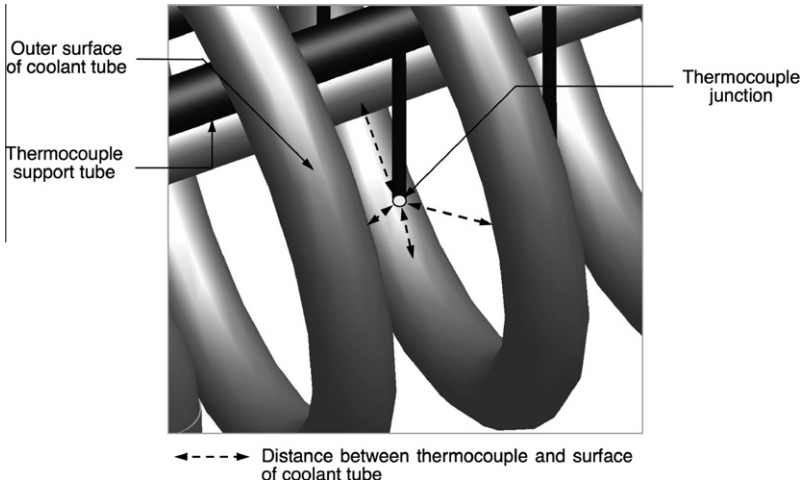

Fig. 9. Schematic showing different distances of thermocouple from the surface of the coolant tube, which are used to identify the shortest distance used in Fig. 10.

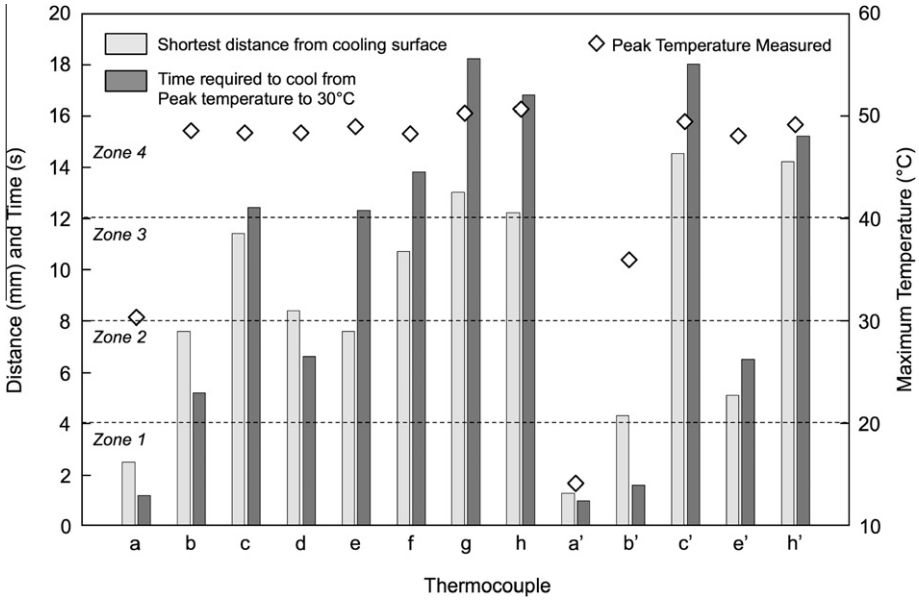

Fig. 10. Plot of shortest distance to coolant tube, peak temperature, and time required to cool from peak temperature to 30 °C for each thermocouple location.

coolant tube proximity, and, therefore, cooling effectiveness for a given thermocouple location.

4.3. Hydriding Reaction

Fig. 10 shows, for each thermocouple, both the thermocouple's shortest distance and the time it took the metal hydride at the same location to cool down from its peak temperature (designated by a diamond symbol) to 30 °C. Notice how all thermocouples with a shortest distance of 5 mm or greater reached about the same peak temperature around 50 °C, while those closer than 5 mm reached much lower peak temperatures. This is particularly the case for thermocouple *a*′, which almost touches the coolant tube, reaching a peak temperature of only 16 °C. Fig. 10 suggests a strong correlation between cooling time and the shortest distance, with locations farthest away requiring the longest cooling time. Overall, the thermocouples can be loosely divided into four different zones of decreasing cooling rate based on their shortest distance to the cooling surface, 0–4 mm, 4–8 mm, 8–12 mm, and over 12 mm as shown in Fig. 10. The temperature profiles measured by thermocouples in each of these zones are similar and can be grouped together. One thermocouple from each zone is therefore selected to represent its zone and the temperatures recorded by only four thermocouples are shown in the bottom plot of Fig. 8.

The four thermocouples *b*′, *d*, *c* and *g* are located at increasing distances from the coolant tube, ranging from 2 to 13 mm, and each represents one of the four zones. Hence, the remainder of this study will use the temperature profiles measured by only these four thermocouples to assess the overall performance of the heat exchanger, including comparisons with computational results in the second part of this study [21].

4.4. Dehydriding reaction

The hydriding reaction was deemed complete once the flow meter indicated that no more hydrogen was flowing into the pressure vessel. At this point, the pressure vessel was depressurized by closing the hydrogen supply valve and opening the vent valve. The vent regulator was programed to allow controlled venting of the hydrogen gas, generally between 0.1 and 0.3 g/s. As the pressure decreased, the hydride temperature began to drop. Dehydriding commenced around 80 bar, 38 min into the test, before which the temperature drop was purely the result of depressurization. During the endothermic dehydriding process, the metal hydride temperature dropped to as low as −48 °C as shown in Fig. 8. Locations that reached the highest temperatures during hydriding, also reached the lowest temperatures during dehydriding. In test 1, the coolant temperature was not increased during dehydriding, which caused the dehydriding reaction to be slow. Just before 50 min into the test, the vent valve was closed when the pressure reached 7 bar, at which point the metal hydride temperature started increasing because the coolant was at a relatively warmer temperature of 2.5 °C. However, dehydriding continued, causing the hydrogen gas released from the metal hydride to be trapped in the pressure vessel, which in turn, caused the pressure to increase slightly. At 62 min, the vent valve was again opened and closed quickly, which allowed the residual hydrogen gas to be released. The pressure vessel was then sealed and maintained at 7 bar. Once the metal hydride reached uniform temperature, the pressure vessel was isolated from the hydrogen and coolant lines, at which point the test was complete.

4.5. Hydriding data comparison

As indicated earlier, the present study is focused on the hydriding process. Hence, experimental data for only the hydriding portion of the tests are discussed and later compared with the computational results in the second part of this study [21] to assess the heat exchanger's performance. Temperatures measured by thermocouples *b*′, *d*, *c* and *g* are designated as T1, T2, T3 and T4, respectively.

The hydriding data from the four tests performed are shown in Figs. 11–14, and operating conditions for these tests are listed in Table 1. Shown in each figure are profiles for pressure inside the pressure vessel, flow rate of hydrogen gas entering the pressure vessel, and temperatures recorded by thermocouples T1–T4. Fig. 11 shows the hydriding results for test 1, in which the coolant was maintained at 2.5 °C, the lowest of all tests. During a minute-long linear pressurization ramp, hydrogen gas flowed into the pressure vessel at around 2.5 g/s. Once the peak pressure of 280 bar was reached, the hydrogen flow became intermittent. This behavior can be explained as follows. As the hydride absorbed

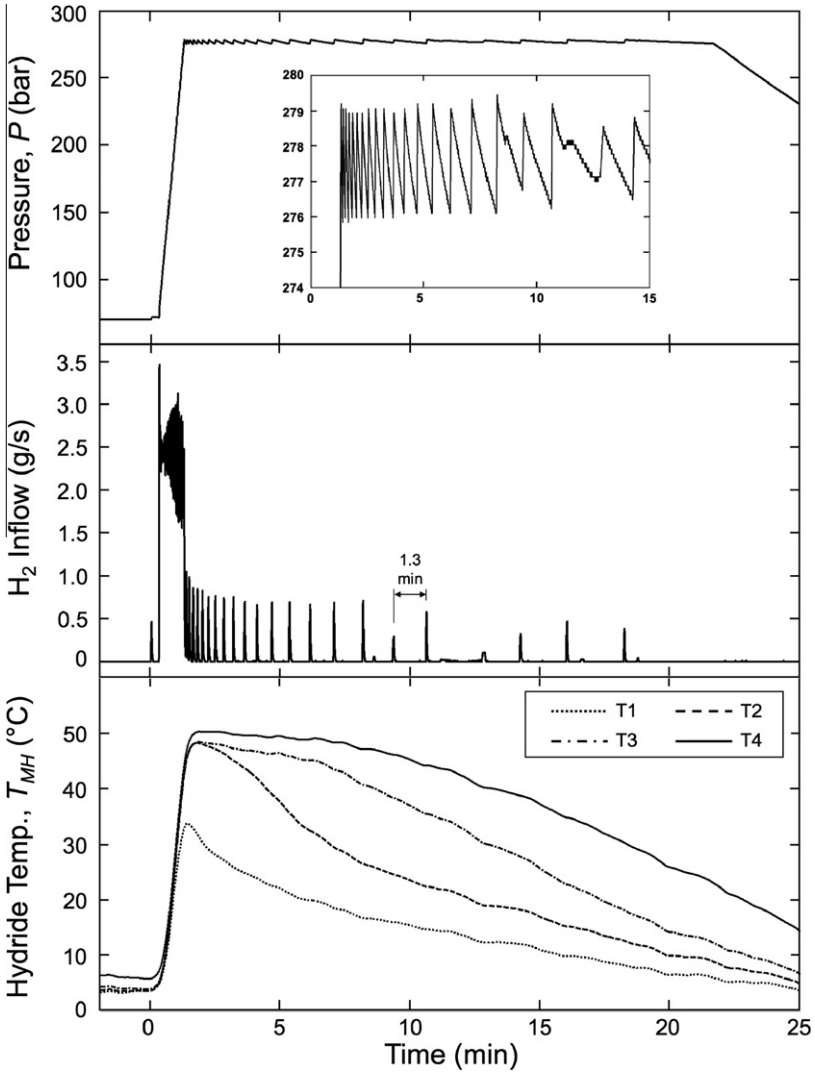

Fig. 11. Hydriding data for test 1.

the hydrogen, the pressure in the vessel dropped momentarily. When the pressure dropped by 3 bar, the programable supply regulator allowed more hydrogen flow to the pressure vessel to restore the desired maximum pressure of 280 bar. This cycle of pressure drop followed by introduction of additional hydrogen by the regulator was repeated several times, taking the form of pressure fluctuations and spikes in the hydrogen flow rate as shown in the top and middle plots, respectively, in Fig. 11. As the hydriding reaction proceeded further, the frequency of pressure fluctuations and hydrogen spikes decreased, especially as the reaction neared completion. At the end of the pressurization ramp (at 1 min), hydrogen was introduced every few seconds, but 10 min into the pressurization, the frequency of hydrogen introduction dropped to 1.3 min. After about 11 min, the frequency as well as the amount of hydrogen gas introduced in every spike decreased even further, indicating the completion of most part of the hydriding reaction. It must be noted that, at this stage, pressure drop in the pressure vessel is partly due to the hydriding reaction but also due to the cooling provided by the heat exchanger. The hydrogen supply valve was kept open until 20 min to ensure that the hydriding reaction is complete and to allow metal hydride particles to reach uniform temperature, after which the vent valve was opened to start the dehydriding experiments. Shown in the bottom plot are the profiles of metal hydride temperatures measured at four locations during hydriding. Thermocouples T1–T4 are situated in order of increasing distance from the coolant tube surface, T1 being the closest and T4 the farthest. The distances of T1, T2, T3 and T4 from the tube are 4.3, 8.4, 11.4, and 13.0 mm, respectively. Only T4 recorded a peak temperature of 50 °C, which is the temperature corresponding to an equilibrium pressure of 280 bar. T2 and T3 measured peak temperatures of 48 °C, while T1 measured a much lower peak temperature of 32 °C. Also, T1 and T2 saw a drop in temperature as soon as the pressurization ramp was completed. However, T3 and T4 maintained their peak temperatures for a while before they started dropping in temperature. These temperature profiles show the importance of both proximity to the cooling surface and the maximum hydride thickness criterion used in the heat exchanger design.

Fig. 12 shows the hydriding data for test 2 in which the coolant was maintained at 21 °C, the highest of all tests. The increased coolant temperature reduced the rate of heat removal from the metal hydride, which greatly reduced hydriding reaction rate. Compared to test 1, the temperatures recorded in test 2 were higher due mostly to the higher initial metal hydride temperature. Both the frequency of hydrogen introduction and the amount of introduced hydrogen were smaller in test 2 as a result of slower hydriding rate. As the reaction proceeded further, a continuous increase in the time between successive spikes of

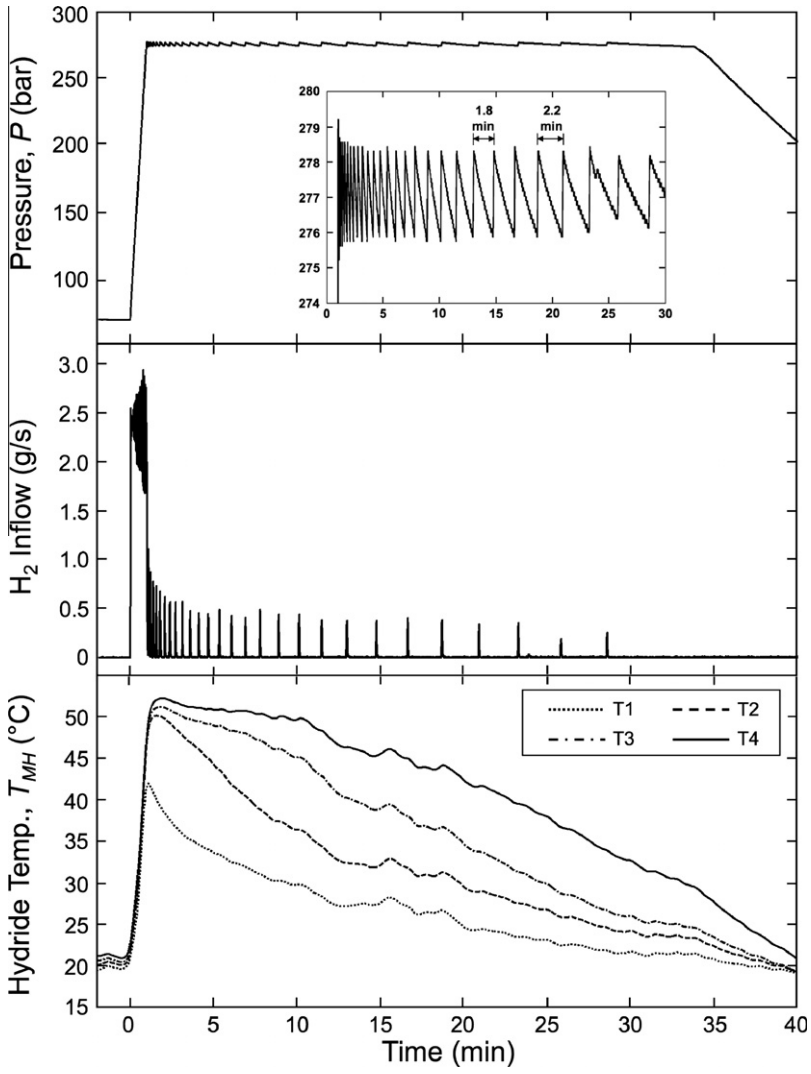

Fig. 12. Hydriding data for test 2.

hydrogen introduction was observed. 20 min into the reaction, the time between consecutive spikes increased to 2.2 min, indicating that most of the hydride particles had completed the hydriding reaction.

Fig. 13 shows the hydriding data for test 3, which was performed in absence of any coolant flow. Here, heat could only be dissipated very slowly through the walls of the pressure vessel to the ambient air. Unlike tests 1 and 2, in test 3, all thermocouples in test 3 reached the same peak temperature of 50 °C. The temperatures remained around 50 °C for 10 min before beginning to slowly decrease. Without the coolant flow in test 3, heat transfer and hydriding rate were highly compromised. This is evident from the over 50% reduction in the frequency of hydrogen introduction compared to test 2. Past 30 min, the time between successive hydrogen spikes was more than 3 min. Furthermore, the hydriding reaction for test 3 took more than 40 min to complete compared to 20 min for test 2.

While the pressurization rate was identical for tests 1, 2 and 3 (70–280 bar in 60 s), a slower pressurization rate of 70–280 bar in 300 s was adopted in test 4. During the pressurization ramp in test 4, hydrogen flowed into the pressure vessel at 1.2 g/s as shown in Fig. 14. A change in the slope of the temperature profiles is observed about 120 s into the pressure ramp, indicating the commencement of the hydriding reaction. Until then, due to the slow pressurization rate, the pressure was not high enough to exceed the equilibrium pressure and initiate the reaction. Also, due to the slow pressurization, the rate of reaction was slower and peak metal hydride temperatures lower than those for test 1, which had similar operating conditions but faster pressurization rate. With the slow pressurization rate, the hydriding reaction for test 4 was completed in about 15 min, a bit longer than test 1.

In all four experiments, the rate of hydriding decreased as the reaction progressed. This is due to two reasons, (a) self-limiting nature of the hydriding reaction (hydriding inherently slows as it approaches completion) and (b) higher metal hydride temperatures due to the exothermic reaction. Metal hydride particles close to the coolant tube cooled faster and completed hydriding earlier due to higher heat transfer rates. The importance of low coolant temperatures to increasing hydriding rate can be gauged by comparing data from tests 1 and 2. In test 2, with the coolant at 21 °C, the reaction time (>20 min) is almost twice that of test 1, where the coolant was at 2.5 °C. In absence of any coolant flow during test 3, the time to complete hydriding was even longer, more than 40 min. Under similar operating conditions for tests 1 and 4, pressurizing the hydride at a slower rate (70–280 bar in 300 s in test 4 compared to 70–280 in 60 s in test 1), increased reaction rate by only 2–3 min. These test prove that reaction rate is far more sensitive to coolant temperature than to pressurization rate.

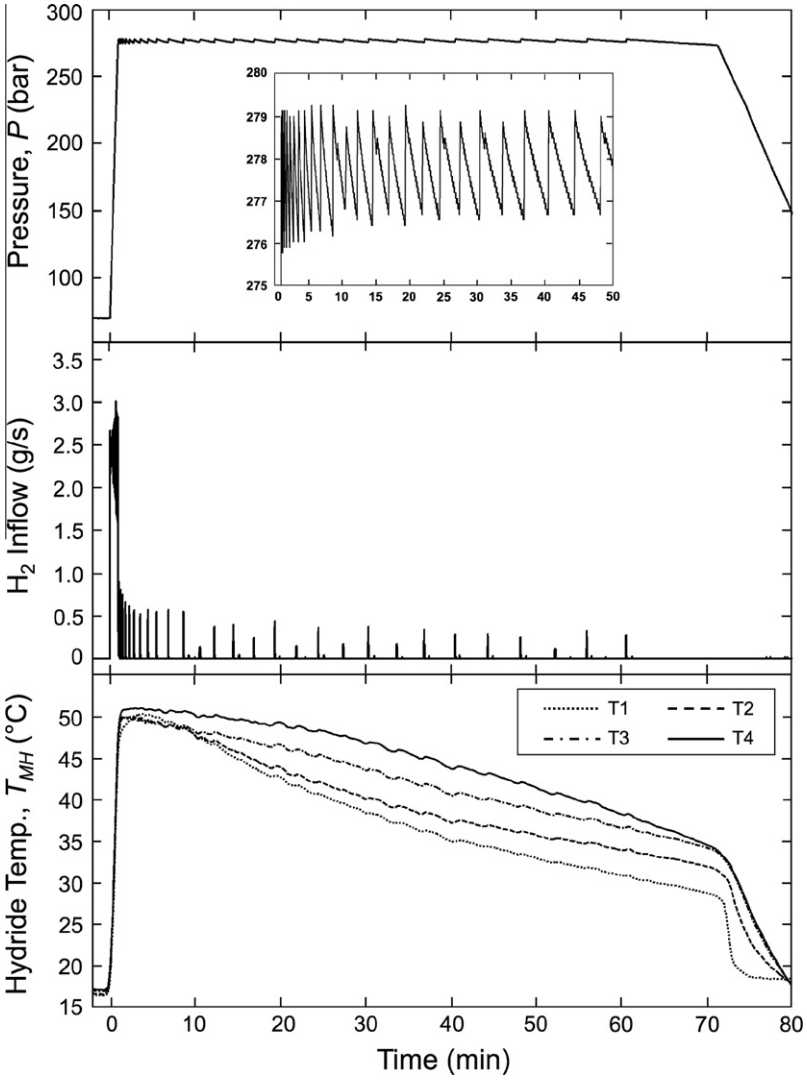

Fig. 13. Hydriding data for test 3.

The second part of this study [21] will present a 3D computational heat transfer model of the storage vessel and heat exchanger, and compare the model predictions to the present experimental data.

5. Conclusions

This paper explored the cooling performance of a simple coiled-tube heat exchanger for hydrogen storage systems utilizing High-Pressure Metal Hydride (HPMH). The primary function of this heat exchanger is to remove the large amounts of heat released when the hydrogen is charged into the storage system. The key premise in the heat exchanger design proposed in this study is to ensure proximity of the coolant tube to hydride particles everywhere inside the storage system. The heat exchanger tested in this study ensured that all hydride particles were within 15 mm from the coolant tube. Key conclusions from the study are as follow.

1. In hydrogen fuel cell applications such as those being considered for automobiles, the heat exchanger in a HPMH storage system must be compact, lightweight, and allow hydrogen to be filled within reasonable time. The present coiled heat exchanger occupies only 7% of the storage pressure vessel volume, providing ample space for the metal hydride and, therefore, hydrogen storage. This is a significant improvement in storage capacity compared to previous modular tube-fin heat exchanger design by the authors, where the heat exchanger occupied 29% of the pressure vessel volume [19–20]. However, increased storage capacity causes the fill time (defined as time required to complete 90% of the hydriding reaction) to increase due to the reduced heat transfer performance. Under similar operating conditions, the fill time using the present coiled heat exchanger is about twice as long as that of the modular tube-fin heat exchanger.
2. The distance of metal hydride particles from the coolant tube has the most dominant influence on the rate of hydriding, with particles closer to the tube completing their hydriding reaction sooner. This influence is aided by the 3D geometry of the coiled coolant tube.
3. Coolant temperature has the most significant impact on the rate of hydriding of all operating conditions. Decreasing the coolant temperature from 21 to 2.5 °C reduced hydriding time from 21 to 12 min.
4. Slow pressurization results in lower hydride temperatures due to smaller heat generation rates. Slowing the pressurization ramp from 60 to 300 s increased hydriding time by 3 min.

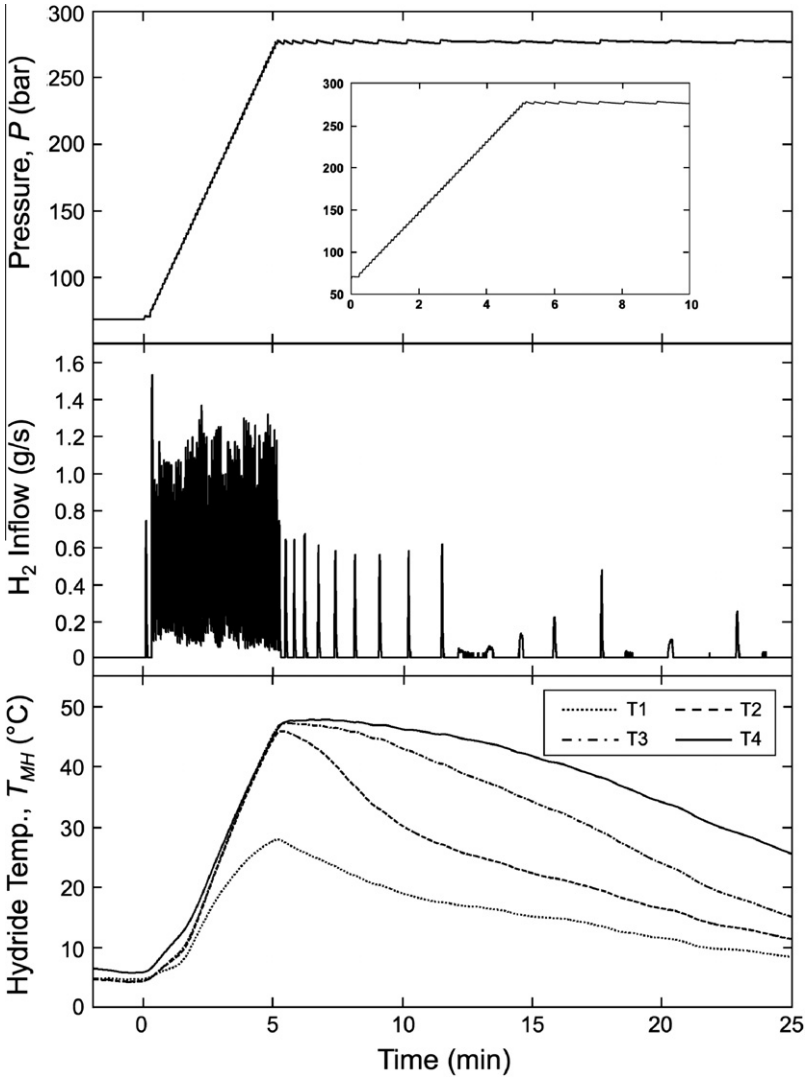

Fig. 14. Hydriding data for test 4.

5. The hydriding reaction is extremely slow in the absence of coolant flow. By relying solely on slow conduction through the pressure vessel walls and external natural convection, some hydride locations took an hour to drop by 10 °C from peak temperature, and the hydriding time increased to 40 min, over four times longer than with low temperature coolant. This demonstrates the overall effectiveness of the present heat exchanger at reducing fill time by 75% while occupying only 7% of the storage pressure vessel volume.

References

[1] N. Takeichi, H. Senoh, T. Yokota, H. Tsuruta, K. Hamada, H. Takeshita, H. Tanaka, T. Kiyobayashi, T. Takano, N. Kuriyama, Hybrid hydrogen storage vessel a novel high pressure hydrogen storage vessel combined with hydrogen storage material, Int. J. Hydrogen Energ. 28 (2003) 1121–1129.
[2] S.M. Aceves, G.D. Berry, J. Martinez-Frias, F. Espinosa-Loza, Vehicular storage of hydrogen in insulated pressure vessels, Int. J. Hydrogen Energ. 31 (2006) 2274–2283.
[3] S.M. Aceves, F. Espinosa-Loza, E. Ledesma-Orozco, T.O. Ross, A.H. Weisberg, T.C. Brunner, O. Kircher, High-density automotive hydrogen storage with cryogenic capable pressure vessels, Int. J. Hydrogen Energ. 35 (2010) 1219–1226.
[4] G. Walker, Solid-State Hydrogen Storage: Materials and Chemistry, Woodhead publishing, Cambridge, England, 2008.
[5] A. Zuttel, Materials for Hydrogen Storage, Materials Today 6 (2003) 24–33.
[6] Y. Kaplan, Effect of design parameters on enhancement of hydrogen charging in metal hydride reactors, Int. J. Hydrogen Energ. 34 (2009) 2288–2294.
[7] H. Dhaou, A. Souahlia, S. Mellouli, F. Askri, A. Jemni, S. Ben Nasrallah, Experimental study of a metal hydride vessel based on a finned spiral heat exchanger, Int. J. Hydrogen Energ. 35 (2010) 1674–1680.
[8] F. Askri, M. Ben Salah, A. Jemni, S. Ben Nasrallah, Optimization of hydrogen storage in Metal-Hydride tanks, Int. J. Hydrogen Energ. 34 (2009) 897–905.
[9] T. Pourpoint, V. Velagapudi, I. Mudawar, Y. Zheng, T. Fisher, Active cooling of a metal hydride system for hydrogen storage, Int. J. Heat Mass Transfer 53 (2010) 1326–1332.
[10] M. Visaria, I. Mudawar, T. Pourpoint, S. Kumar, Parametric study of heat transfer and kinetics parameters influencing the design of heat exchangers for hydrogen storage in high-pressure metal hydrides, Int. J. Heat Mass Transfer 53 (2010) 2229–2239.
[11] D. Mori, K. Hirose, Recent challenges of hydrogen storage technologies for fuel cell vehicles, Int. J. Hydrogen Energ. 34 (2009) 4569–4574.
[12] E. Poirier, A. Dailly, Thermodynamic study of the adsorbed hydrogen phase in Cu-based metal-organic frameworks at cryogenic temperatures, J. Phys. Chem. C 112 (2008) 13047–13052.
[13] A. Chaise, P. De Rango, P. Marty, D. Fruchart, Experimental and numerical study of a magnesium hydride tank, Int. J. Hydrogen Energ. 35 (2010) 6311–6322.
[14] M. Melnichuk, N. Silin, H.A. Peretti, Optimized heat transfer fin design for a metal-hydride hydrogen storage container, Int. J. Hydrogen Energ. 34 (2009) 3417–3424.
[15] S. Mellouli, F. Askri, H. Dhaou, A. Jemni, S. Ben Nasrallah, A novel design of a heat exchanger for a metal-hydrogen reactor, Int. J. Hydrogen Energ. 32 (2007) 3501–3507.
[16] S. Mellouli, F. Askri, H. Dhaou, A. Jemni, S. Ben Nasrallah, Numerical simulation of heat and mass transfer in metal hydride hydrogen storage tanks for fuel cell vehicles, Int. J. Hydrogen Energ. 35 (2010) 1693–1705.
[17] F. Laurencelle, J. Goyette, Simulation of heat transfer in a metal hydride reactor with aluminum foam, Int. J. Hydrogen Energ. 32 (2007) 2957–2964.

[18] M. Botzung, S. Chaudourne, O. Gillia, C. Perret, M. Latroche, A. Percheron-Guegan, P. Marty, Simulation and experimental validation of a hydrogen storage tank with metal hydrides, Int. J. Hydrogen Energ. 33 (2008) 98–104.
[19] M. Visaria, I. Mudawar, T. Pourpoint, Enhanced heat exchanger design for hydrogen storage using High-Pressure Metal Hydride – Part 1. Design methodology and computational design, Int. J. Heat Mass Transfer 54 (2011) 413–432.
[20] M. Visaria, I. Mudawar, T. Pourpoint, Enhanced heat exchanger for hydrogen storage using High-Pressure Metal Hydride – Part 2. Experimental results, Int. J. Heat Mass Transfer 54 (2011) 424–432.
[21] M. Visaria, I. Mudawar, Coiled-tube heat exchanger for High-Pressure Metal Hydride hydrogen storage systems – part 2. Computational model, International Journal of Heat and Mass transfer 55 (2012) 1796–1806.
[22] U. Mayer, M. Groll, W. Supper, Heat and mass transfer in metal hydride reaction beds: Experimental and theoretical results, J. Less-Common Metals 131 (1987) 235–244.